

# Resonances of an optical $\lambda/4$ nano-antenna probed by single molecule fluorescence

*Tim H. Taminiou<sup>1</sup>, Robert J. Moerland<sup>2</sup>, Frans B. Segerink<sup>2</sup>, Laurens Kuipers<sup>2,3</sup>*

*and Niek F. van Hulst<sup>\*1,4</sup>*

ICFO – Institut de Ciències Fotòniques, Av. Canal Olímpic, Castelldefels (Barcelona), 08860, Spain, *and* Applied Optics Group, MESA+ Institute for NanoTechnology, University of Twente, P.O.Box 217, 7500AE Enschede, the Netherlands.

\*Niek.vanHulst@ICFO.es

**(Received date)**

<sup>1</sup>ICFO – Institut de Ciències Fotòniques

<sup>2</sup>Applied Optics Group, MESA+

<sup>3</sup>FOM Institute for Atomic and Molecular Physics (AMOLF), Kruislaan 407, 1098SJ Amsterdam, the Netherlands

<sup>4</sup>ICREA – Institució Catalana de Recerca i Estudis Avançats, 08015 Barcelona, Spain

## **ABSTRACT**

We present a resonant optical  $\lambda/4$  nano-antenna positioned at the end of a metal-coated glass fiber near-field probe. Antenna resonances, excitation conditions and field localization are directly probed in the near field by single fluorescent molecules and compared to finite integration technique simulations. It is shown that, for the right antenna length and local excitation conditions, antenna resonances occur that lead to a highly localized field near the antenna apex. Direct mapping of this field with single fluorescent molecules reveals a spatial localization of 25 nm, demonstrating the importance of such antennas for nanometer resolution optical microscopy.

## **MAIN TEXT**

Antennas play an essential role as transmitters and receivers in our modern wireless society. The charge movements they support efficiently link propagating electromagnetic fields to localized fields. Radiation from a distant source can be concentrated in a local volume, vice versa a localized excitation can be efficiently coupled into directed radiation. The efficiency of an antenna depends critically on its resonances, as dictated by the operation frequency and by the shape, material and dimensions of the antenna. Only recently antennas are experimentally explored in the optical domain, where they are crucial to surpass the fundamental diffraction limit. Properly engineered antennas will play a decisive role in the manipulation of light on the nanometer scale, such as control and optimization of emissive systems,<sup>1-3</sup> nano-fabrication,<sup>4</sup> optical manipulation and characterization,<sup>5-7</sup> integrated opto-electronic devices and, as shown in this letter, sub-wavelength optical microscopy.<sup>8,9</sup>

So far most research has focused on optical antennas fabricated on planar substrates, restricting their applications. Resonances and coupling effects of such antennas have been investigated thoroughly by linear far-field spectroscopy<sup>10-12</sup> and by exploiting non-linear responses,<sup>13</sup> such as two photon luminescence.<sup>14-16</sup> Unfortunately these characterization techniques do not allow a direct local measurement of the electric field. More insight can be obtained using single emitters, such as fluorescent molecules, which are well-defined and direct “point” probes of both local field amplitude and direction.<sup>9,17</sup> To accomplish this, either the emitter or the antenna has to be mounted on a scanning probe. In near-field scanning optical microscopy (NSOM) scattering type probes are used, which exploit the local field enhancement near a sharp tip.<sup>18-20</sup> Such probes could be labeled antennas, however their infinite size does not support geometrical resonances.<sup>21</sup> Only a few examples of finite-size probe-based antennas have been demonstrated, a gold nanoparticle attached to a glass probe<sup>22-24</sup> and an aluminum bowtie antenna.<sup>2</sup>

All antennas mentioned are illuminated from the far field in a large, at best diffraction limited, focus. The extended illuminated area adds a background contribution to the antenna response. The resulting background problem can be overcome by detection of nonlinear processes<sup>19,25</sup> or by modulation techniques.<sup>20</sup> However, the large illuminated area is unacceptable in fluorescence detection where photobleaching is a primary drawback. Conventional NSOM aperture probes<sup>26</sup> provide a background-free localized excitation volume, but the obtainable field confinement is limited in practice by the low throughput of sub-wavelength apertures. Frey *et al.*<sup>27</sup> combined scattering and aperture probes by placing a sharp metal tip next to a sub-wavelength aperture. They showed that high optical and topographical resolution can be obtained with reduced background illumination due to the local excitation through the aperture.<sup>28</sup> In principle intensity is sacrificed to reduce the background contribution.

In this letter we present a probe-based nano-antenna, tuned to resonance by controlling its length. The nano-antenna is excited by placing it in the near field of an aperture fiber probe, providing low background illumination. The antenna response is simulated using the Finite Integration Technique (FIT),<sup>29</sup> giving insight in the antenna excitation conditions and resonance behavior and showing the equivalence of the antenna with a standard radio  $\lambda/4$ -antenna. The antenna near field is mapped by single fluorescent molecules in NSOM experiments, thus directly probing the antenna resonances and the resulting field localization down to  $\sim 25$  nm.

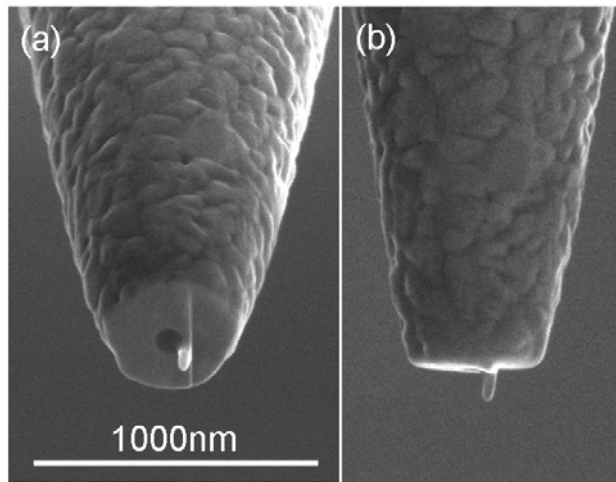


Figure 1. A probe-based nano-antenna (SEM images), (a) viewed from a  $52^\circ$  angle and (b) side view.

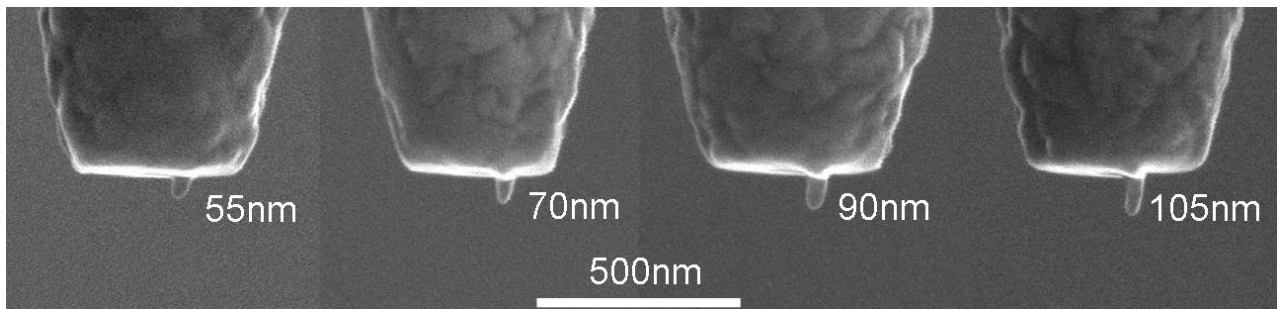


Figure 2. Tuning the antenna length to investigate its resonance. Length:  $55\pm 5$  nm,  $70\pm 5$  nm,  $90\pm 5$  nm and  $105\pm 5$  nm (SEM images).

Probe-based antennas are fabricated in a way similar to conventional aperture probes.<sup>26</sup> Sharp glass tips are created by heat-pulling single-mode (633 nm wavelength) glass fibers using a commercial pipette puller (Sutter P2000). Next the probes are coated all-around by evaporation with a few nanometer thick chromium adhesion layer and  $\sim 150$  nm of aluminum. Aluminum is chosen for its short optical penetration depth. This also implies its optical behavior is relatively close to a perfect electrical conductor (PEC), which favors comparison to the radio antenna analogue. Finally, by Focused Ion (Ga<sup>+</sup>) Beam (FIB) milling under two different angles, a well-defined elongated antenna ( $\sim 50$  nm width,  $\sim 20$  nm radius of curvature) is created on a flat end-face next to a circular aperture (100 nm diameter). Figure 1 shows SEM images of a resulting probe-based antenna. To investigate the antenna resonances the antenna length has been controllably varied from 30 nm to 140 nm. Typical examples are shown in Figure 2. The well-defined antenna probes allow us to investigate their resonant response and compare the experimental behavior directly to FIT simulations.

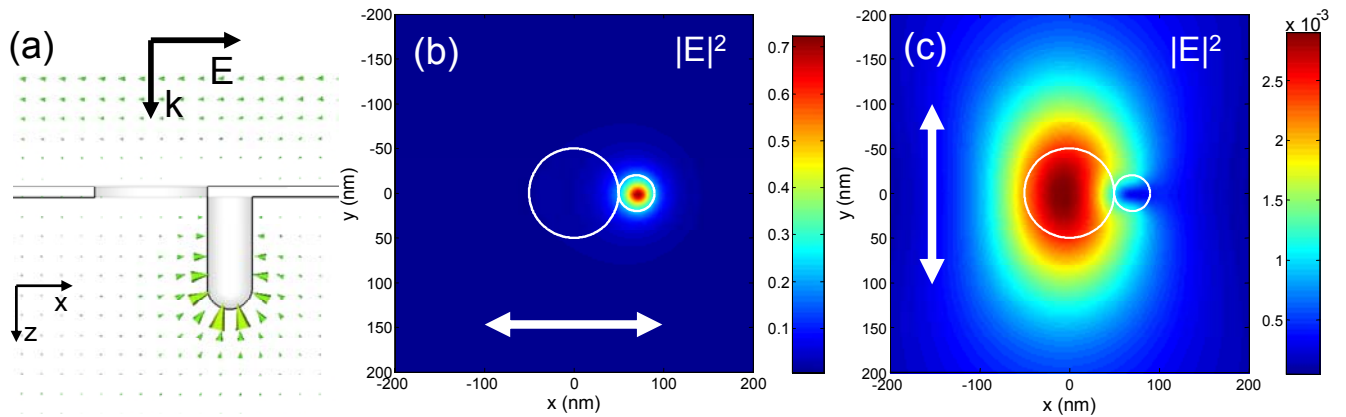


Figure 3. Field localization and polarization dependent excitation of the antenna (FIT simulations). (a) A cross-section of the antenna structure and the resulting field (instantaneous; full phase cycle available online). (b, c) The time-averaged field intensity normalized to the incoming wave intensity is evaluated in a plane 10 nm below the antenna apex for two

polarization directions of the incoming plane wave (see arrows); (b) in the direction of the antenna and (c) the direction perpendicular to that. The large circle represents the aperture (radius 50 nm), the small one the antenna (radius 20 nm).

3D FIT simulations are performed using commercial software (CST Microwave Studio).<sup>30</sup> The antenna is modeled as cylinder with a rounded apex placed next to an aperture (100 nm diameter) in an infinitely large 10 nm thick PEC plate. A cross-section of the configuration is shown in Figure 3a. A plane wave ( $\lambda = 514$  nm) with variable polarization illuminates the plate from the top. It is anticipated that the antenna is driven by applying a field component along the antenna axis, the z-direction. For an aperture probe it has been shown experimentally<sup>9,17,31,32</sup> and theoretically<sup>33,34</sup> that this component is present at the aperture edges in the direction of the incoming polarization. The antenna is therefore ideally positioned at the edge of the aperture. Figures 3b and 3c show the field intensity evaluated in a plane 10 nm below the antenna apex. For the polarization in the direction of the line through the centers of the aperture and the antenna (Figure 3b) a field component along the antenna axis is present. The antenna is excited and a highly localized enhanced field forms near the antenna apex. The full width at half maximum (FWHM) of the intensity pattern is 27 nm for the conditions in Figure 3b. For the perpendicular polarization, no such field is formed and only the two orders of magnitude weaker intensity distribution originating from the aperture is found (Figure 3c).

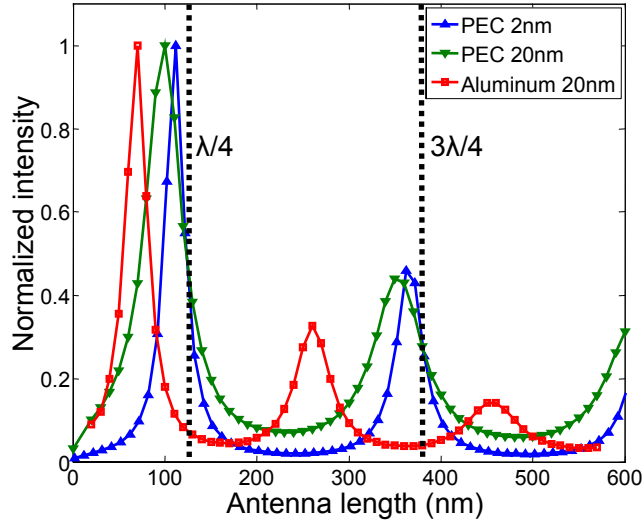


Figure 4. Calculated antenna resonances. The field intensity 10 nm below the antenna apex normalized on the maximum against the antenna length for different antennas: perfect electrical conducting (PEC) radius 2 nm (blue line, upward triangles) and 20 nm (green line, downward triangles), aluminum radius 20 nm (red line, circles).  $\lambda = 514$  nm.

The antenna resonances are determined by the size, shape and material parameters of the antenna. Figure 4 illustrates the resonances by varying the length for three antennas of different radius and material properties, all at  $\lambda = 514$  nm. For a 2 nm radius PEC antenna the imaginary part of the input impedance of the antenna goes to zero for lengths slightly less than uneven multiples of  $\lambda/4$  (115 nm, 365 nm); resonance occurs and a strong field is formed at the antenna apex,  $90^\circ$  out-of-phase with the driving field (see full phase cycle online). The phase lag of a quarter optical cycle is a clear signature of resonant response. The even multiples of  $\lambda/4$  in length are anti-resonances resulting in minimum field strength. The behavior found is equivalent to that of one of the most commonly used antennas in mobile communication, the  $\lambda/4$ -antenna or monopole-antenna, which consists of a thin metal cylinder placed on a ground plane that acts as a mirror for the field.<sup>35</sup> The probe-based antenna is a similar  $\lambda/4$ -antenna, however illuminated locally by the aperture instead of collecting far-field radiation.

Increasing the radius of the antenna shifts the resonance to shorter length ( $\sim 100$  nm) and increases the bandwidth (or peak width),<sup>35</sup> as illustrated in Figure 3 for a 20 nm radius PEC antenna. Aluminum is not a PEC at optical frequencies. For  $\lambda = 514$  nm the complex dielectric constant of aluminum is  $\epsilon = -31.3 + 8.0i$ , as determined by fitting a Drude model to experimental values.<sup>36</sup> For an aluminum antenna the resonance shifts to even shorter length ( $\sim 70$  nm). Although the free space wavelength is kept constant, the wavelength of the standing-wave charge oscillation at resonance along/in the antenna is shortened both for thicker and imperfect-metal antennas; optical antennas have resonances at shorter length than equivalent thin radio-wave antennas. Note that the second resonance of the aluminum antenna (at a length equal to  $\frac{3}{4} \lambda$  of the charge oscillation) coincides with the first anti-resonance for a thin PEC antenna (at  $\lambda/2$  of the free wave).

To experimentally verify the properties of the nano-antenna, single fluorescent molecules are used to map the local antenna field. To this end samples consisting of isolated DiI-molecules in a 10-20 nm thick PMMA layer are prepared by spin coating. The single-molecule samples are scanned underneath the antenna probe using a near-field scanning optical microscope with shear-force feedback, as described in detail earlier.<sup>37</sup> In order to control the excitation polarization at the probe's end-face, the polarization of the laser light ( $\lambda = 514$  nm, Ar<sup>+</sup> line) is adjusted before being coupled into the probe fiber and characterized after being emitted from the probe. The collected molecular fluorescence is filtered from the exciting laser light, split into two branches by a polarizing beam splitter and detected by photon counting avalanche photodiodes (APDs). This way the polarization of the fluorescence is monitored and information about the orientation of the molecular emission dipole is obtained.

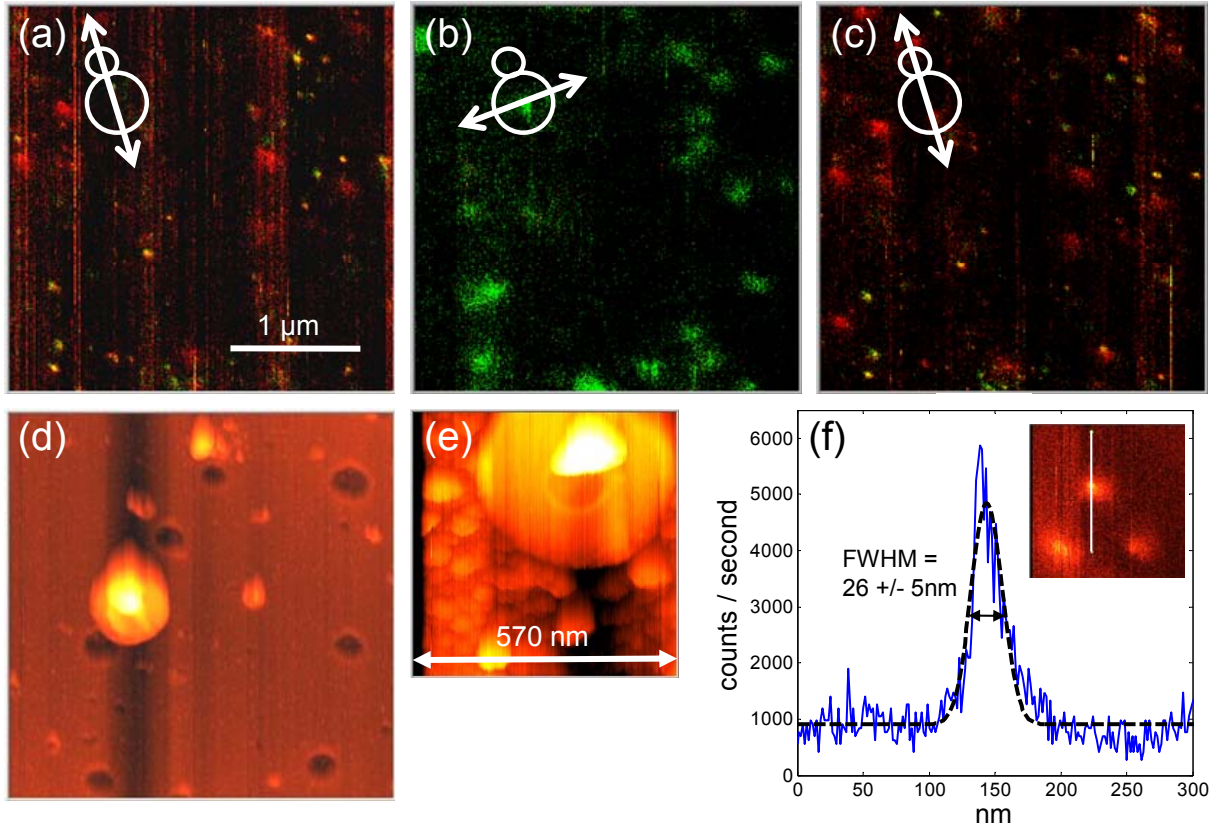


Figure 5. Single molecule NSOM experiments revealing narrow features for the right excitation polarization, indicating a highly localized field. Fluorescence (a,b,c,f) and topographical results (d,e) for an antenna of  $85 \pm 5$  nm length. The incoming polarization is in the direction of the antenna for (a) and (c), perpendicular to that for (b) (see inset, antenna: small circle, aperture: larger circle, polarization: arrow). The color scaling represents the polarization of the collected fluorescence. Red is vertical, green horizontal.<sup>37</sup> (d) Topography obtained simultaneously with scan (a). (e) Close up of a topographic antenna feature for a different probe. (f) Cross-section of the intensity profile of one of the molecules in (a) and Gaussian fit (black dashed line) showing a width of  $26 \pm 5$  nm.

Figures 5a, b and c show the single molecule fluorescence response for an 85 nm long antenna. For polarization of the light in the direction of the antenna (Figure 5a) tiny single molecular

patterns are found together with several weaker larger spots originating from the illumination from the aperture. When the polarization direction is rotated by 90° (Figure 5b) only large weak spots are found, with emission polarization mainly along the incident direction. By restoring the polarization (Figure 5c) the original image with small features is recovered, proving that the effect is purely optical. Indeed, as predicted by simulations, a highly localized field is formed at the antenna apex for the right polarization of the excitation. Figure 5f shows a cross-section from a close-up scan of one of the molecules in Figure 5a. A width (FWHM) of 26 +/- 5 nm is found for a Gaussian fit, in good agreement with the value found for the simulated intensity pattern. This confirms that the field is highly localized and bound to the antenna dimensions. The narrow field confinement effectively demonstrates the strength of antenna based high resolution NSOM. In contrast to our data, Frey *et al.*<sup>28</sup> reported molecular patterns with dark spots in the center of the patterns for molecules directly on mica, which has been attributed partly to quenching of the fluorescence by the metal tip. We use molecules embedded in a 10-20 nm polymer layer, thick enough to minimize quenching influences. Indeed, in general we do not observe such dark spots and characteristic patterns are shown in the inset of Figure 5f.

The single molecule fluorescence is not correlated to the simultaneously recorded surface topography (Figure 5d), confirming that the narrow optical response is not height induced. Interestingly, topographical responses that provide valuable information on the antenna structure can be observed. Figure 5d shows a large feature caused by the convolution of the probe with a surface particle that is higher than the antenna length. A clearer example, for another probe, is presented in Figure 5e. The antenna, the flat end-face of the probe and even the aperture can clearly be recognized. The orientation of the antenna with respect to the aperture can directly be determined. The topographic height gives an independent and precise measurement of the

antenna length taken *in situ* during the actual measurement and thus allows continuous monitoring of the antenna length.

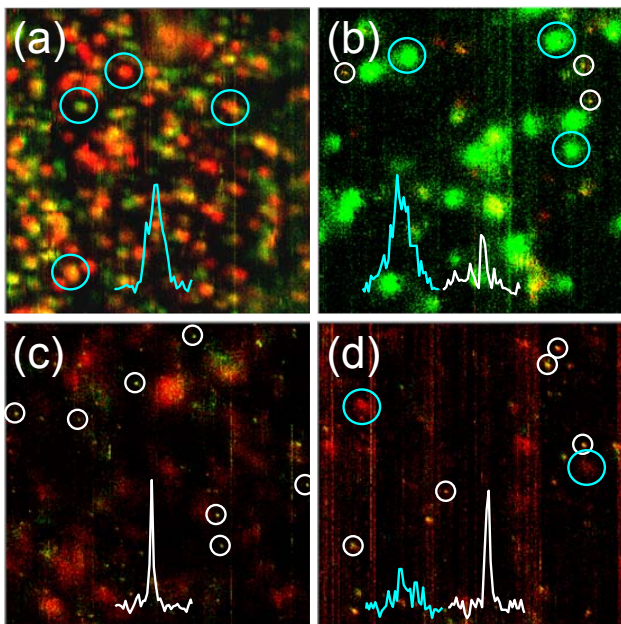


Figure 6. Single molecule fluorescence response for antennas of increasing length. Narrow features, indicating a highly localized field and thus resonance, are found for 70-90nm long antennas. Antenna lengths of (a) 30 +/- 5 nm, (b) 50 +/- 5 nm, (c)75+/-5 nm (d) 85+/-5 nm. All images are 3  $\mu\text{m}$  x 3  $\mu\text{m}$ . The insets are characteristic cross-sections (all 400 nm in length) of the correspondingly marked molecular patterns. The patterns associated with the antenna (FWHM = ~25nm) are marked with small white circles, those with the aperture field (FWHM > 80 nm) with large blue circles.

To directly probe the influence of antenna resonances, single molecules have been excited by antennas of different lengths. For a total of 18 probes we obtained a data set of single molecule fluorescence responses. Figure 6 shows four examples with increasing antenna length. Very short antennas (30 nm, Figure 6a) only give single molecule patterns with dimensions comparable to the aperture diameter (FWHM > 80 nm), like for conventional aperture probes.<sup>17</sup> Slightly longer

antennas (50 nm, Figure 6b) exhibit additional signs of excitation resulting from the presence of the antenna. However, antennas with a length between 70 and 90 nm result in clearly resolvable narrow molecular features (FWHM =  $\sim 25$  nm) (Figures 6c and 6d), proving the presence of a strong highly-localized field. When antennas longer than 90 nm were fabricated, they generally did not result in any convincing fluorescence response, indicating that antennas of those lengths are not effective. Antennas long enough to reach the second resonance ( $\sim 260$  nm) predicted in Figure 4 could not be reproducibly fabricated. Note that, for a static field enhancement effect, the “lightning rod” effect, the shortest antenna is expected to show the strongest response, since it is located closer to the aperture and thus effectively in a stronger field. However, we do not observe the strongest response for the shortest (30-50 nm) antennas. The results actually show a strong highly confined field for antenna lengths around 70-90nm, indicating dynamic resonance. Although structural variations from probe to probe hinder quantitative analysis, the trend revealed by the results is in good agreement with the resonant behavior predicted in simulations (figure 4). Moreover the value found for the maximum antenna efficiency (70-90nm) is in agreement with resonant length obtained from simulations (70nm), confirming that the resonant length of the optical antenna is shortened compared to the equivalent radio  $\lambda/4$ -antenna.

In conclusion, resonances and field localization of probe-based nano-optical  $\lambda/4$  antennas have been directly demonstrated by single fluorescent molecule experiments. Clear polarization-dependent excitation conditions are observed that agree with FIT simulations. By controlling the antenna length we have revealed a trend that indicates a resonance behavior in good qualitative agreement with simulations, which shows that the finite thickness and material parameters of the optical antennas reduce the effective resonance length compared to equivalent radio antennas. The highly localized field formed at the antenna apex for the right excitation conditions and

resonant antenna length is shown to be confined laterally within 25 nm FWHM, demonstrating the importance of such antennas for nanometer resolution optical microscopy.

## ACKNOWLEDGEMENTS

This work has benefited from support by the Specific Target Research Project (STRP) ASPRINT (NMP-CT-2003-001601) in the 6<sup>th</sup> Framework Program of the European Community. This work is part of the research program of the Stichting voor Fundamenteel Onderzoek der Materie (FOM), which is financially supported by the Nederlandse Organisatie voor Wetenschappelijk Onderzoek (NWO). Finally we thank Computer Simulation Technology (CST), Darmstadt, Germany, for constructive feedback on the use of Microwave Studio.

## SUPPORTING INFORMATION

Antenna field calculations: full phase cycles and intensity images at resonance for different antennas. This material is available free of charge via the Internet at <http://pubs.acs.org>.

## REFERENCES

1. Greffet, J. -J. *Science* **2005**, 308, 1561.
2. Farahni, J.N.; Pohl, D.W.; Eisler, H.-J.; Hecht, B. *Phys. Rev. Lett.* **2005**, 95, 017402.
3. Gersen, H.; Garcia-Parajo, M. F.; Novotny, L.; Veerman, J. A.; Kuipers, L.; van Hulst, N. F. *Phys. Rev. Lett.* **2001**, 85, 5312.
4. Sundaramurthy, A.; Schuck, P. J.; Conley, N. R.; Fromm, D. P.; Kino, G. S.; Moerner, W. E. *Nano Lett.* **2006**, 6, 355.
5. Novotny, L.; Bian, R. X.; Xie, X. S. *Phys. Rev. Lett.* **1997**, 79, 645.

6. Hartschuh, A.; Sánchez, E. J.; Xie, X. S.; Novotny, L. *Phys. Rev. Lett.* **2003**, 90, 095503.
7. Fromm, D. P.; Sundaramurthy, A.; Kinkhabwala, A.; Schuck, P. J.; Kino, G. S.; Moerner, W. E. *J. Chem. Phys.* **2006**, 124, 061101.
8. Pohl, D. W.; Denk, W.; Lanz, M. *Appl. Phys. Lett.* **1984**, 44, 651.
9. Betzig, E; Chichester, R. J. *Science* **1993**, 262, 1422.
10. Fromm, D. P.; Sundaramurthy, A.; Schuck, J.; Kino, G.; Moerner, W. E. *Nano Lett.* **2004**, 4, 957.
11. Crozier, K. B.; Sundaramurthy, A.; Kino, G. S.; Quate, C. F. *J. Appl. Phys.* **2003**, 94, 4632.
12. Rechberger, W.; Hohenau, A.; Leitner, A.; Krenn, J. R.; Lamprecht, B.; Aussenegg, F. *R. Opt. Commun* **2003**, 220, 137.
13. Mühlischlegel, P.; Eisler, H. -J.; Martin, O. J. F.; Hecht, B.; Pohl, D. W. *Science* **2005**, 308, 1607.
14. Bouhelier, A.; Bachelot, R.; Lerondel, G.; Kostcheev, S.; Royer, P.; Wiederrecht, G. P. *Phys. Rev. Lett.* **2005**, 95, 267405.
15. Schuck, P. J.; Fromm, D. P.; Sundaramurthy, A.; Kino, G. S.; Moerner, W. E. *Phys. Rev. Lett.* **2005**, 94, 017402.
16. ten Bloemendal, D.; Ghenuche, P.; Quidant, R.; Cormack, I. G.; Loza-Alvarez, P.; Badenes G. *Plasmonics* **2006**, 1, 41.

17. Veerman, J.A.; Garcia-Parajo, M. F.; Kuipers, L.; van Hulst, N. F. *J. Microsc.* **1999**, 194, 477.
18. Zenhausern, F.; Martin, Y.; Wickramasinghe, H. K. *Science* **1995**, 269, 1083.
19. Sánchez, E. J.; Novotny, L.; Xie, X. S. *Phys. Rev. Lett.* **1999**, 82, 4014.
20. Gerton, J. M.; Wade, L. A.; Lessard, G. A.; Ma, Z.; Quake, S. R. *Phys. Rev. Lett.* **2004**, 93, 180801.
21. Krug II, J. T.; Sánchez, E. J.; Xie, X. S. *J. Chem. Phys.* **2002**, 116, 10895.
22. Kalkbrenner, T.; Håkanson, U.; Schädle, A.; Burger, S.; Henkel, C.; Sandoghdar, V. *Phys. Rev. Lett.* **2005**, 95, 200801.
23. Anger, P.; Bharadwaj, P.; Novotny, L. *Phys. Rev. Lett.* **2006**, 96, 113002.
24. Kühn, S.; Håkanson, U.; Rogobete, L.; Sandoghdar, V. *Phys. Rev. Lett.* **2006**, 97, 017402.
25. Stöckle, R.M.; Suh, Y.D.; Deckert, V.; Zenobi, R. *Chem. Phys. Lett.* **2000**, 318, 131.
26. Veerman, J.A.; Otter, A. M.; Kuipers, L.; van Hulst, N. F. *Appl. Phys. Lett.* **1998**, 72, 3115.
27. Frey, H. G.; Keilmann, F.; Kriele, A.; Guckenberger, R. *Appl. Phys. Lett.* **2002**, 81, 5030.
28. Frey, G. F.; Witt, S.; Felderer, K.; Guckenberger, R. *Phys. Rev. Lett.* **2004**, 93, 200801.
29. Weiland, T. *Electron. Commun. AEU* **1977**, 31, 116.

30. CST Microwave Studio 5.1, [www.cst.com](http://www.cst.com)
31. Naber, A.; Molenda, D.; Fischer, U. C.; Maas, H. -J.; Höppener, C.; Lu, N.; Fuchs, H. *Phys. Rev. Lett.* **2002**, 89, 210801.
32. Moerland, R. J.; van Hulst, N. F.; Gersen, H.; Kuipers, L. *Optics Express* **2005**, 13, 1604.
33. Bouwkamp, C. J. *Phillips Res. Report* **1950**, 5, 321; *ibid.* **1950**, 5, 401.
34. Martin, O. J. F.; Paulus, M. *J. Microsc.* **2002**, 205, 147.
35. Balanis, C. A. *Antenna Theory: Analyses and Design*, 3<sup>rd</sup> ed, **2005**. ISBN: 0-471-66782-X.
36. (a) Hass, G.; Waylonis, J. E. *J. Opt. Soc. Am.* **1960**, 50, 1133. (b) Schultz, L. G.; Tangherlini, F. R. *J. Opt. Soc. Am.* **1954**, 44, 362. (c) Schultz, L. G. *J. Opt. Soc. Am.* **1954**, 44, 357.
37. Ruiter, A. G. T.; Veerman, J. A.; Garcia-Parajo, M. F.; van Hulst, N. F. *J. Phys. Chem. A* **1997**, 101, 7318.